Letter

King and second-King plots with optimized sensitivity for lithium ions

G. W. F. Drake, Harvir S. Dhindsa, and Victor J. Marton*
Department of Physics, University of Windsor, Windsor, Ontario, Canada N9B 3P4

(Received 16 September 2021; accepted 18 November 2021; published 6 December 2021)

King plots constructed from combinations of mass-weighted atomic isotope shifts provide a sensitive technique to search for electron-neutron interactions beyond the standard model mediated by a light boson. Using high-precision variational wave functions in Hylleraas coordinates, we present a comprehensive survey of all possible King plots arising from states of Li^+ up to principal quantum number $n = 10$ and angular momentum $L = 7$ in order to identify the ones most sensitive to new physics. A major limitation in previous work due to second-order mass polarization is eliminated by the introduction of a second-King plot defined in terms of second differences. The residual theoretical uncertainty is then of the order of $\alpha^2(\mu/M)^3 \sim 0.4$ Hz, where α is the fine-structure constant and μ is the reduced electron mass for a nucleus of mass M. Test results are presented for the $^A Li^+$ isotope sequence with $A = 6, 7, 8, 9, 11$ and are compared with other methods, including the Yb^+ case recently studied both experimentally and theoretically. It is shown that the second-King plots for Li^+ have about the same sensitivity to new physics as the Yb^+ case for boson masses up to about 10 keV, and nuclear size uncertainties (including nuclear polarization) are suppressed. This greatly extends the sensitivity to new physics for light two-electron systems.

DOI: 10.1103/PhysRevA.104.L060801

I. INTRODUCTION

King plots have long been used to analyze isotope shift measurements in atoms and extract information about the nucleus [1]. Ideally, a linear relationship should result when appropriately mass-scaled transition frequencies are plotted against one another across a range of isotopes with the same nuclear charge Z. However, recently, there has been a great deal of interest in using King plots to search for new physics beyond the standard model (BSM) [2–4]. In particular, light bosons may exist that couple electrons to neutrons, resulting in an additional Yukawa-like interaction that varies from one isotope to the next according to the number of neutrons [5]. The resulting interaction could possibly reveal itself as a deviation from linearity of the King plot.

Two recent high-precision experiments have been performed with the aim of searching for new physics BSM. The first used the King plot to study S-D quadrupole transitions in isotopes of Yb^+ [6], and the second, in effect, studied isotope shifts in the fine-structure splittings of Ca^+ [7]. The Yb^+ experiment showed a 3σ deviation from linearity in the King plot, which could potentially be a signal of new physics BSM or other nuclear structure effects, while the Ca^+ experiment showed no significant deviation from linearity. Flambaum *et al.* [8] proposed that nuclear polarization effects may account for the Yb^+ anomaly.

Most work to date has been based on relatively heavy atomic systems such as these. The main point of the present paper is to show that there is an important scope for future experiments on light two-electron ions such as Li+ and Be^{++}.

In the case of Li^+, there are five experimentally accessible isotopes whose isotope shifts have all been extensively studied before (for the case of neutral Li) in connection with measurements of the nuclear charge radius [9,10] and, more recently, for $^6Li^+$ and $^7Li^+$ [11,12]. An advantage of working with two-electron systems is that high-precision atomic structure calculations are readily done [13] to facilitate the interpretation of measured isotope shifts.

An additional electron-neutron interaction mediated by light bosons would lead to a Yukawa-type potential of the form [5]

$$V_{m_\phi} = \frac{N_I y_e y_n}{4\pi r} e^{-\gamma r}, \tag{1}$$

where $\gamma = m_\phi c/\hbar$ for a hypothetical light boson of mass m_ϕ, $y_e y_n/(4\pi)$ is a coupling constant, and N_I is the number of neutrons for isotope I, analogous to $Ze^2/(4\pi\epsilon_0)$ for the electron-nucleus interaction. Since it is only the change in N_I between isotopes that contributes to the relative isotope shift, there is no particular advantage in working with heavy isotopes with large N_I, at least for boson masses below about 10 keV. However, a disadvantage of working with light isotopes is that higher-order terms proportional to $(\mu/M)^2$ and higher must be taken into account in a King-plot analysis, where μ is the electron reduced mass and M is the nuclear mass. Such terms arise, for example, from mass polarization in the electronic structure and must be taken into account. In this work, we show that by taking second differences, a second-King or "super-King" plot can be constructed to eliminate terms of order $(\mu/M)^2$.

In the present work, we report the results of an extensive scan of transitions among the Rydberg states of Li^+ covering all states up to principal quantum number $n = 10$ and angular

*gdrake@uwindsor.ca

momentum $L = 7$ (K states) in order to identify the most favorable cases for possible experiments. In the following section, the conventional King plot is briefly summarized and then extended to the second-King plot, and the influence of a hypothetical electron-neutron interaction is discussed. This is followed by a brief description of the computational methods and a presentation of the results.

II. THE KING PLOT AND SECOND-KING PLOT

Let i and j denote two atomic states and a be a particular isotope. The transition frequency between states i an j can then be expanded in the form

$$\nu_a^{ij} = U^{ij} + V^{ij}\left(\frac{\mu}{M}\right)_a + W^{ij}\left(\frac{\mu}{M}\right)_a^2 + \cdots + C^{ij}\bar{r_a^2}, \tag{2}$$

where $U^{ij} = (E^i - E^j)/\hbar$ is the transition frequency for an infinitely heavy point nucleus (including relativistic and QED corrections), V^{ij} denotes contributions from both the normal and specific isotope shifts due to mass polarization, W^{ij} denotes second-order contributions from the same sources, and the last term, $\bar{r_a^2}$, is the lowest-order correction due to the finite nuclear charge radius squared. The coefficient C^{ij} is given (in lowest order) by

$$C^{ij} = \frac{2\pi Ze^2}{3}\sum_k [\langle\delta(\mathbf{r}_k)\rangle_i - \langle\delta(\mathbf{r}_k)\rangle_j] \tag{3}$$

summed over the electron coordinates r_k and so is determined by the change in electron density at the nucleus for states i and j, independent of the isotope to a good approximation. Further nuclear structure and finite-mass corrections may also be important [2,8], but the above is sufficient for the purposes of the present discussion. The normal procedure in constructing a King plot is to define the King coordinate

$$\eta_{ab}^{ij} = \frac{\nu_a^{ij} - \nu_b^{ij}}{\left(\frac{\mu}{M}\right)_a - \left(\frac{\mu}{M}\right)_b}. \tag{4}$$

Then, with the definitions

$$F_{ab} = \left(\frac{\mu}{M}\right)_a + \left(\frac{\mu}{M}\right)_b, \tag{5}$$

$$G_{ab} = \frac{\bar{r_a^2} - \bar{r_b^2}}{\left(\frac{\mu}{M}\right)_a - \left(\frac{\mu}{M}\right)_b}, \tag{6}$$

the King coordinate can be written in the form

$$\eta_{ab}^{ij} = V^{ij} + W^{ij}F_{ab} + C^{ij}G_{ab}. \tag{7}$$

The slope of the King plot for a pair of transitions $i'j'$ plotted on one axis and ij plotted on the other and for a sequence of isotopes a, b, and c is defined by

$$S = \frac{\eta_{ac}^{i'j'} - \eta_{ab}^{i'j'}}{\eta_{ac}^{ij} - \eta_{ab}^{ij}}. \tag{8}$$

For heavy ions, the normal procedure is to ignore the W^{ij} term in Eq. (4). The factors of $G_{ac} - G_{ab}$ in the numerator and denominator then cancel, leaving

$$S = \frac{C^{i'j'}}{C^{ij}} \tag{9}$$

for all isotope pairs.

For light ions, the W^{ij} term can also be eliminated by forming the second-King coordinate

$$\kappa_{abc}^{ij} = \frac{\eta_{ab} - \eta_{ac}}{\left(\frac{\mu}{M}\right)_b - \left(\frac{\mu}{M}\right)_c}. \tag{10}$$

Then, with the definition

$$\begin{aligned} Q_{abc} = {} & \frac{\bar{r_a^2}}{\left[\left(\frac{\mu}{M}\right)_a - \left(\frac{\mu}{M}\right)_b\right]\left[\left(\frac{\mu}{M}\right)_a - \left(\frac{\mu}{M}\right)_c\right]} \\ & + \frac{\bar{r_b^2}}{\left[\left(\frac{\mu}{M}\right)_b - \left(\frac{\mu}{M}\right)_a\right]\left[\left(\frac{\mu}{M}\right)_b - \left(\frac{\mu}{M}\right)_c\right]} \\ & + \frac{\bar{r_c^2}}{\left[\left(\frac{\mu}{M}\right)_c - \left(\frac{\mu}{M}\right)_a\right]\left[\left(\frac{\mu}{M}\right)_c - \left(\frac{\mu}{M}\right)_b\right]} \end{aligned} \tag{11}$$

Eq. (10) becomes

$$\kappa_{abc}^{ij} = W^{ij} + C^{ij}Q_{abc} + O(\mu/M). \tag{12}$$

If the $O(\mu/M)$ corrections due to higher-order mass polarization are neglected, then factors of $Q_{abc} - Q_{abd}$ cancel from the numerator and denominator of the second-King slope defined by

$$S^{(2)} = \frac{\kappa_{abc}^{i'j'} - \kappa_{abd}^{i'j'}}{\kappa_{abc}^{ij} - \kappa_{abd}^{ij}}, \tag{13}$$

leaving $S^{(2)} = \frac{C^{i'j'}}{C^{ij}}$, which is identical to Eq. (9) for the standard King slope. However, since the Q's are larger than the G's by a factor of the order of $(\mu/M)^{-1} \sim 10^4$, the cancellation is more nearly exact for the case of the second-King plot, thereby suppressing nuclear size uncertainties by about this factor. The disadvantage, of course, is that one needs a sequence five isotopes instead of four to look for a change in slope due to new physics BSM.

III. EXTENDED KING PLOT TO SEARCH FOR NEW PHYSICS BSM

Suppose now that there is an additional interaction of the form of Eq. (1). Since this term enters the analysis in parallel with the finite-nuclear-size term Q_{abc}, the modified second-King coordinate becomes

$$\kappa_{abc}^{ij} = W^{ij} + C^{ij}Q_{abc} + \Upsilon^{ij}N_{abc}, \tag{14}$$

where, in parallel with Eq. (3),

$$\Upsilon^{ij} = \frac{y_e y_n}{4\pi}\sum_k [\langle e^{-r_k/\lambda_m}/r_k\rangle_i - \langle e^{-r_k/\lambda_m}/r_k\rangle_j] \tag{15}$$

and, in parallel with Eq. (11),

$$\begin{aligned} N_{abc} = {} & \frac{N_a}{\left[\left(\frac{\mu}{M}\right)_a - \left(\frac{\mu}{M}\right)_b\right]\left[\left(\frac{\mu}{M}\right)_a - \left(\frac{\mu}{M}\right)_c\right]} \\ & + \frac{N_b}{\left[\left(\frac{\mu}{M}\right)_b - \left(\frac{\mu}{M}\right)_a\right]\left[\left(\frac{\mu}{M}\right)_b - \left(\frac{\mu}{M}\right)_c\right]} \\ & + \frac{N_c}{\left[\left(\frac{\mu}{M}\right)_c - \left(\frac{\mu}{M}\right)_a\right]\left[\left(\frac{\mu}{M}\right)_c - \left(\frac{\mu}{M}\right)_b\right]}, \end{aligned} \tag{16}$$

where N_a, N_b, and N_c are the neutron numbers for isotopes a, b, and c, respectively. Note that $N_{abc} = 0$ if $\{N_a, N_b, N_c\}$ are all

equal, so it depends only on the change in neutron number. As with the Q's in Eq. (12), the N's are enhanced by a factor of $(\mu/M)^{-1} \sim 10^4$.

For brevity, we define $\Delta Q_{cd} = Q_{abc} - Q_{abd}$ and $\Delta N_{cd} = N_{abc} - N_{abd}$. Once again, the W^{ij} term cancels from the slope of the second-King plot, resulting in

$$S^{(2)} = \frac{C^{i'j'}\Delta Q_{cd} + \Upsilon^{i'j'}\Delta N_{cd}}{C^{ij}\Delta Q_{cd} + \Upsilon^{ij}\Delta N_{cd}} \simeq \frac{C^{i'j'}}{C^{ij}}\left[1 + \left(\frac{\Upsilon^{i'j'}}{C^{i'j'}} - \frac{\Upsilon^{ij}}{C^{ij}}\right)\frac{\Delta N_{cd}}{\Delta Q_{cd}}\right], \tag{17}$$

assuming in the second line that the Υ^{ij} term is small so that the denominator can be expanded into the numerator. Finally, if the isotope d is replaced by a fifth isotope e, then the change in slope is

$$\Delta S^{(2)}_{de} = \frac{C^{i'j'}}{C^{ij}}\left(\frac{\Upsilon^{i'j'}}{C^{i'j'}} - \frac{\Upsilon^{ij}}{C^{ij}}\right)\left(\frac{\Delta N_{ce}}{\Delta Q_{ce}} - \frac{\Delta N_{cd}}{\Delta Q_{cd}}\right). \tag{18}$$

This shows a clear factorization into a part determined by the nuclear properties represented by the last factor and a part determined by the electronic wave function represented by the first two factors. A nonzero value for the middle factor would represent a signal of new physics BSM. The 1-Hz sensitivity is then defined as the value for $y_e y_n$ for which $\Delta S^{(2)}_{de}/S^{(2)} = \Delta S^{(2)}_{1\mathrm{Hz}}/S^{(2)}$, where $\Delta S^{(2)}_{1\mathrm{Hz}}$ is the uncertainty induced in $S^{(2)}$ by uncertainties of 1 Hz in each of the four isotope shift measurements, added in quadrature.

IV. DETAILED CALCULATIONS FOR Li^+

The purpose of this section is to summarize the method used to calculate matrix elements and isotope shifts for Li^+. The starting point is to find solutions to the Schrödinger equation with the mass polarization term $\mathbf{p}_1 \cdot \mathbf{p}_2/M$ included explicitly in the Hamiltonian. High-precision solutions are found by using variational wave functions in Hylleraas coordinates of the form [13–15]

$$\Psi = c_0\Psi_0 + \sum_{ijk}^{i+j+k\leqslant\Omega}\left[\underbrace{c^{(\mathrm{A})}_{ijk}\varphi_{ijk}(\alpha_\mathrm{A},\beta_\mathrm{A})}_{\text{A sector}} + \underbrace{c^{(\mathrm{B})}_{ijk}\varphi_{ijk}(\alpha_\mathrm{B},\beta_\mathrm{B})}_{\text{B sector}}\right], \tag{19}$$

where Ψ_0 is the screened hydrogenic term $\psi_{1s}(r_1, Z)\psi_{nL}(r_2, Z-1)$, $Z-1$ is the screened nuclear charge of the Rydberg nL electron, and the basis functions $\varphi_{ijk}(\alpha, \beta)$ are defined by

$$\varphi_{ijk}(\alpha,\beta) = r_1^i\, r_2^j\, r_{12}^k\, e^{-\alpha r_1 - \beta r_2}\, \mathcal{Y}^M_{l_1,l_2,L}(\hat{r}_1,\hat{r}_2) \pm \text{exchange}.$$

The quantity $\mathcal{Y}^M_{l_1,l_2,L}(\hat{r}_1,\hat{r}_2)$ represents a vector-coupled product of spherical harmonics of angular momenta l_1 and l_2 to form a state with total angular momentum L and component M. The parameter $\Omega = (i+j+k)_{\max}$ controls the size of the basis set. Different nonlinear parameters α_A, β_A and α_B, β_B are used for the asymptotic (A) and short-range (B) sectors, respectively, as determined by calculating analytically the four derivatives $\partial E/\partial\alpha_X$ and $\partial E/\partial\beta_X$ and finding zeros using Newton's method [14,15]. An advantage of these doubled basis sets is their compactness and numerical stability such that standard quadruple precision (approximately 32 decimal digits) in FORTRAN is sufficient, even for the largest basis sets with up to 1566 terms. In addition, the accuracy does not deteriorate significantly for the higher-lying Rydberg states up to $n = 10$ and $L = 7$.

The remaining step is to calculate matrix elements of the δ-function and Yukawa potential for each state. For matrix elements of $\delta(\mathbf{r}_1) + \delta(\mathbf{r}_2)$, there is an asymptotic expansion that becomes extremely accurate for $L \gtrsim 3$ [16]. Relativistic and QED corrections were also calculated, as extensively described previously [15,17,18]. These terms are needed to calculate the total transition frequencies, but they do not significantly affect the slopes of the second-King plots since the leading nonvanishing term is of the order of $(\alpha)^2(\mu/M)^3 \sim 10^{-17}$ a.u. (0.4 Hz). QED corrections are smaller still and can be neglected in the second-King analysis. Detailed wave functions, matrix elements, and total energies for these states are available online [19].

V. RESULTS

In order to identify the optimized King plots most sensitive to a light boson, we conducted a survey of all possible King plots involving singlet and triplet transitions (including intercombination transitions) up to $n = 10$ and $L = 7$ (K-states). Counting both singlets and triplets and ignoring fine structure, there is a total of 103 states. The number of possible unique King plots is therefore $N(N-1)[N(N-1)-2]/8 = 13\,794\,378$. The results that follow cover all of these, with the exception of combinations involving the $7\ ^{1,3}I$-$10\ ^{1,3}H$ transitions. For these, there is an accidental cancellation of matrix elements of the δ-function in the lowest order in μ/M, making the nuclear size term anomalously small. Nuclear size and structure uncertainties are thereby suppressed. These transitions form a special case that will be discussed separately in a future publication.

As shown in Table I, the second-King plots with the highest sensitivity all involve transitions starting from principle quantum number $n = 2$ in the limit of small γ (i.e., small boson mass) and $n = 1$ for large γ. The upper states all terminate at $n = 10$ for small γ, but this just represents the asymptotic limit for the highest n in the sample space of states. In other words, the same transitions with $n = 9$ and $n = 8$ have only slightly less sensitivity, and so the choice is more a matter of experimental convenience. In this limit, the Yukawa potential is almost the same as a Coulomb potential over atomic dimensions, but as γ increases, the exponential cutoff occurs at progressively shorter distances. Correspondingly, the optimum value of n for the upper state decreases toward $n = 2$ with increasing γ. The transition from the low-γ regime to the high-γ regime occurs over a relatively narrow range around $\gamma = 0.5$. At the other extreme, the $2\ ^3P$-$8\ ^3S/8\ ^3G$-$8\ ^3H$ combination has a sensitivity of only 2.6×10^{-8} in the small-γ limit. The Supplemental Material [20] gives a more extensive tabulation for small and intermediate γ, including the 15 unique second-King plots formed by the four states with $n = 2$. For these, the sensitivities are an order of magnitude worse than for the optimized transitions in Table I.

TABLE I. Transitions with the highest sensitivity to electron-neutron interactions for different values of the Yukawa parameter γ. The conversion factor from γ to boson mass m_ϕ is $Z\alpha m_e = 11.1868$ keV, with $Z = 3$.

γ (Z/a_0)	King transitions	$y_e y_n$
0.001	$2\,^1S$-$10\,^1S/2\,^3P$-$10\,^1S$	9.6312×10^{-15}
0.002	$2\,^1S$-$10\,^1S/2\,^3P$-$10\,^1S$	9.6465×10^{-15}
0.005	$2\,^1S$-$10\,^1S/2\,^3P$-$10\,^1S$	9.7322×10^{-15}
0.010	$2\,^3P$-$10\,^3S/2\,^1S$-$10\,^1S$	9.9455×10^{-15}
0.020	$2\,^1P$-$5\,^3S/2\,^1P$-$7\,^1S$	1.0363×10^{-14}
0.050	$2\,^1P$-$5\,^3S/2\,^1P$-$7\,^1S$	1.2040×10^{-14}
0.100	$2\,^1P$-$5\,^3S/2\,^1P$-$7\,^1S$	1.5689×10^{-14}
0.200	$2\,^1S$-$10\,^1S/2\,^3P$-$10\,^3S$	2.5312×10^{-14}
0.200	$2\,^1S$-$10\,^3S/2\,^3P$-$10\,^3S$	2.5307×10^{-14}
0.500	$1\,^1S$-$2\,^1S/2\,^3P$-$2\,^3S$[a]	5.4886×10^{-14}
1.000	$1\,^1S$-$2\,^1S/2\,^3S$-$2\,^3P$	1.2293×10^{-13}
2.000	$1\,^1S$-$2\,^1S/2\,^3S$-$2\,^3P$	4.4138×10^{-13}
5.000	$1\,^1S$-$2\,^1S/2\,^3S$-$2\,^3P$	4.8762×10^{-12}
10.000	$1\,^1S$-$2\,^1S/2\,^3S$-$2\,^3P$	4.6078×10^{-11}
20.000	$1\,^1S$-$2\,^1S/2\,^3S$-$2\,^3P$	5.5648×10^{-10}
50.000	$1\,^1S$-$2\,^1S/2\,^3S$-$2\,^3P$	1.9496×10^{-8}
100.00	$1\,^1S$-$2\,^1S/2\,^3S$-$2\,^1P$	2.7815×10^{-7}

[a]For this and the following entries, the strongly forbidden $1\,^1S$-$2\,^3S$ transition has a slightly lower limit.

In the absence of additional bosonic perturbations, the slopes of the King plots should ideally be constant across different choices of isotope pairs. Table II shows the dramatic difference in the variation of slopes between the first-King and second-King cases for the pair of transitions $2\,^1S$-$10\,^1S$ and $2\,^3P$-$10\,^1S$ with the highest sensitivity. Taking ^{7}Li as the common reference isotope, the isotope pairs are (7-6, 7-8), (7-6, 7-9), and (7-6, 7-11) for the three first-King combinations labeled k1, k2, and k3 and (7-6, 7-11, 7-8) and (7-6, 7-11, 7-9) for the two second-King combinations labeled $\mathrm{k1}^{(2)}$ and $\mathrm{k2}^{(2)}$. In the infinite mass limit (first row), all the slopes are perfectly constant and equal to the ratio $C^{i',j'}/C^{i,j}$ as expected. However, with the addition of terms proportional to $(\mu/M)^2$ and higher due to both mass scaling and mass polarization, the slopes k1, k2, and k3 become widely different, while $\mathrm{k1}^{(2)}$ and $\mathrm{k2}^{(2)}$ remain equal to within 12 ppm. Also shown is the uncertainty in the slope due to a nominal ± 1 Hz uncertainty in each of the four input isotope shifts, added in quadrature. The comparison shows that there is a loss of about a factor of 5 in uncertainty of the slope for the second-King plots relative to the first-King plots. The last row shows the uncertainty due to the nuclear radius uncertainties of the five isotopes, added in quadrature. The assumed nuclear charge radii and their uncertainties are the same as in Table VIII of Ref. [10]. As recently discussed by Müller *et al.* [21], the uncertainties in the slopes can be large for first-King plots, but as shown in Table II, the uncertainties are strongly suppressed for the second-King plots. The reason for the suppression follows from the enhanced magnitude of the Q's relative to the G's, as discussed following Eq. (13).

Despite the loss of a factor of 5 in sensitivity, the sensitivity to light bosons of about 1.9×10^{-14} at the 95% confidence level (CL) (i.e., twice the value shown in Table I) is about the same as for the case of Yb^+ recently discussed by Berengut *et al.* [2]. Figure 1 shows a comparison with the regular King-plot limit and the no-mass King plot method of Berengut *et al.* for Yb^+. An important difference is that the present work does not contain a sharp resonancelike peak at around 10 keV. A comparison with other atomic physics methods, such as the H/D isotope shift, neutron scattering, and $g-2$ measurements, is also shown [5]. The comparison with astrophysical limits and fifth-force searches is similar to that discussed previously [2]. These provide much lower bounds on $y_e y_n$, but they are strongly model dependent, so an independent test using atomic physics methods is well justified. Not shown are recent mass limits on a proposed cosmological relaxation of the Higgs field by relaxions [22] and a hypothetical scalar with a finite lifetime that can accommodate the recent KOTO results [23,24], as further discussed in Ref. [2].

The closest previously discussed competitor in a two-electron system [5] is the ^{3}He-^{4}He isotope shift in the $2\,^1S$-$2\,^3S$ [25] and $2\,^3S$-$2\,^3P$ [26,27] transitions around 1557 and 1083 nm, respectively. However, the interpretation in terms of NP is limited by QED uncertainties at the 100-Hz level.

There are two clear disadvantages of working with Li^+. The first is that the optimum transition wavelengths of 87.53 and 89.87 nm lie in the far uv and so are not so easily accessible for high-precision measurements. However, with rapidly improving experimental techniques and synchrotron radiation sources, this problem may be overcome. The second is that all of the isotopes of lithium from ^{6}Li to ^{11}Li contain hyperfine structure, so the center of gravity must be located in order to measure the isotope shift. The advantage of working with a two-electron system such as Li^+ is that high-precision wave functions in Hylleraas coordinates are readily available

TABLE II. Contributions to the slope of the regular King plots k1, k2, and k3 and the second-King (super-King) plots $\mathrm{k1}^{(2)}$ and $\mathrm{k2}^{(2)}$ for the transition pair $2\,^3P_1$-$10\,^3S_1/2\,^3S_1$-$10\,^3S_1$ of Li^+. The nuclear radius uncertainty includes the nuclear polarizability for ^{11}Li (see the text). The last row is the uncertainty in the slope induced by a ± 1-Hz uncertainty in each of the independent isotope shift measurements.

Contribution	k1	k2	k3	$\mathrm{k1}^{(2)}$	$\mathrm{k2}^{(2)}$
Infinite mass limit	–3.453 226	–3.453 226	–3.453 226	–3.453 226	–3.453 226
$(\mu/M)^2 + \cdots$	4.101 441	4.446 124	2.328 237	0.000 153	0.000 082
$(\mu/M)\bar{r}_c^2$	0.000 208	0.000 154	0.000 456	0.000 816	0.000 859
Total	0.648 423	0.993 052	–1.124 533	–3.452 257	–3.452 285
Nuclear radius uncertainty	±0.56	±0.31	±0.06	±0.000 037	±0.000 012
±1 Hz	±0.000 002	±0.000 001	±0.000 001	±0.000 009	±0.000 005

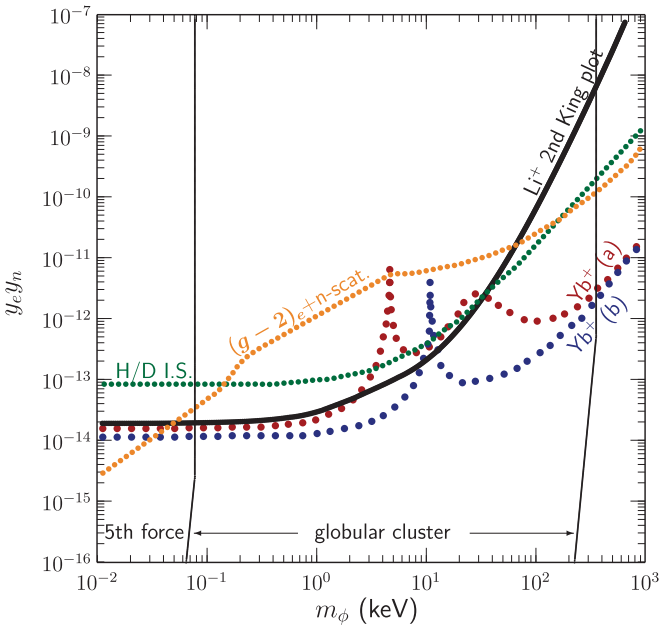

FIG. 1. The 95% CL limits on the coupling constant $y_e y_n$ as a function of boson mass m_ϕ for various methods of measurement. The curves labeled Yb^+ (a) and Yb^+ (b) refer to the King-plot analysis of Berengut *et al.* [2] for (a) a King plot with no mass uncertainty (2DK) and (b) the no-mass generalized King plot (NMK). The solid black curve indicates the present second-King limits for Li^+. The other atomic physics limits come from the H/D isotope shift, neutron scattering, and $(g-2)$ measurements [5]. The astrophysics and fifth-force limits are also shown, as discussed by Berengut *et al.* [2]. Not shown are the recent relaxed-relaxion limits from Ref. [22].

to calculate the hyperfine structure as a function of the nuclear parameters. This was already done in connection with measurements of the nuclear charge radius for all the isotopes of lithium and was recently improved for the cases of $^6Li^+$ and $^7Li^+$ [11]. The main limitation may well be the Zemach effect corresponding to the distribution of magnetic moment across the nucleus. The level widths of the $n = 10$ states were calculated by summing the decay rates over all electric dipole transitions to lower-lying states. The results are 13.33 and 16.16 MHz for $10\,^1S$ and $10\,^3S$ and 229 and 17.4 MHz for $10\,^1P$ and $10\,^3P$, respectively. Except for the $10\,^1P$ state, this is substantially less than the $J = 0 \to 2$ fine-structure splitting of 465.0 MHz for the $10\,^3P_J$ manifold. For high-n Rydberg states, the hyperfine splitting is larger and tends asymptotically to the same splitting as for the ground state of Li^{++}. It ranges from a low of 2.83 GHz for ^{6}Li to a high of 12.8 GHz for ^{7}Li.

For all but ^{11}Li, nuclear polarization effects are small [9] and can be included in the analysis [8]. For the case of ^{11}Li, the energy shift due to nuclear polarization is given by (in atomic units) [28] $E_{\rm pol} = -\alpha mc^2 \langle \sum_i \delta(\mathbf{r}_i) \rangle \alpha_{\rm pol}$, where $\alpha_{\rm pol}$ is the nuclear polarizability, calculated to be [27] $60.9(6.1)\ {\rm fm}^3 = 4.11(41) \times 10^{-13} a_0^3$, where a_0 is the Bohr radius. Since the finite-nuclear-size correction is also proportional to $\langle \sum_i \delta(\mathbf{r}_i) \rangle$, the two can be lumped together to form an effective nuclear charge radius that is the same for all transitions. For the case of ^{11}Li, the nuclear polarizability (including the uncertainty) reduces the effective charge radius from 2.482(14) to 2.316(14) fm. Similarly, higher moments of the nuclear charge distribution can be included in an effective nuclear charge radius since the energy shifts remain approximately proportional to the electron density at the nucleus [2,29].

VI. DISCUSSION

The main point of this paper is to report the results of a broad survey of all possible King plots involving states of Li^+ up to $n = 10$ and $L = 7$, including intercombination transitions, and to identify the ones most sensitive to new physics BSM. The results indicate that the King-plot method applied to light heliumlike ions has a potentially high sensitivity to light bosons mediating an electron-neutron interaction. The use of a second-King plot eliminates second-order mass polarization corrections proportional to $(\mu/M)^2$ if a sequence of five isotopes is available, and the residual corrections of the order of $(\mu/M)^3 \sim 10^{-13}$ can be accurately calculated and included in the analysis if needed. The resulting sensitivity is about the same as for the case of Yb^+ recently discussed in the literature [2]. The method of King-plot analysis also automatically eliminates relativistic recoil and radiative recoil corrections of orders $(Z\alpha)^n \mu/M$ and $(Z\alpha)^n (\mu/M)^2$, with $n = 2, 3, \ldots$. The leading term not included in a purely nonrelativistic calculation is therefore of the order of $(Z\alpha)^2(\mu/M)^3 \sim 10^{-17}$ a.u., or $\sim$0.4 Hz. However, as shown in Table II, relativistic and recoil corrections to the nuclear size term (field shift) could start to become important at the 1-Hz level of accuracy, and the nuclear charge radius uncertainty is about 3 Hz. This is the dominant source of uncertainty. It is particularly significant that the effect of nuclear size uncertainties is strongly suppressed in the second-King plots.

ACKNOWLEDGMENTS

V.J.M. acknowledges support as an undergraduate Outstanding Scholar at the University of Windsor, and H.S.D. received support for this work as a fourth-year undergraduate project. Research support by the Natural Sciences and Engineering Research Council of Canada (NSERC) Grant No. RGPIN-2016-04494 is gratefully acknowledged.

[1] W. H. King, *Isotope Shifts in Atomic Spectra* (Springer Science+Business Media, New York, 1984)

[2] J. C. Berengut, C. Delaunay, A. Geddes, and Y. Soreq, Phys. Rev. Res. **2**, 043444 (2020).

[3] J. C. Berengut, D. Budker, C. Delaunay, V. V. Flambaum, C. Frugiuele, E. Fuchs, C. Grojean, R. Harnik, R. Ozeri, G. Perez, and Y. Soreq, Phys. Rev. Lett. **120**, 091801 (2018)

[4] V. V. Flambaum, A. J. Geddes, and A. V. Viatkina, Phys. Rev. A **97**, 032510 (2018).

[5] C. Delaunay, R. Ozeri, G. Perez, and Y. Soreq, Phys. Rev. D **96**, 093001 (2017).

[6] I. Counts, J. Hur, D. P. L. Aude Craik, H. Jeon, C. Leung, J. C. Berengut, A. Geddes, A. K. Kawasaki, W. Jhe, and V. Vuletić, Phys. Rev. Lett. **125**, 123002 (2020).
[7] C. Solaro, S. Meyer, K. Fisher, J. C. Berengut, E. Fuchs, and M. Drewsen, Phys. Rev. Lett. **125**, 123003 (2020).
[8] V. V. Flambaum, I. B. Samsonov, H. B. T. Tan, and A. V. Viatkina, Phys. Rev. A **103**, 032811 (2021).
[9] W. Nörtershäuser *et al.*, Phys. Rev. A **83**, 012516 (2011).
[10] Z.-T. Lu, P. Mueller, G. W. F. Drake, W. Nörtershäuser, S. C. Pieper, and Z.-C. Yan, Rev. Mod. Phys. **85**, 1383 (2013).
[11] X.-Q. Qi, P.-P. Zhang, Z.-C. Yan, G. W. F. Drake, Z.-X. Zhong, T.-Y. Shi, S.-L. Chen, Y. Huang, and H. Guan, and K.-L. Gao, Phys. Rev. Lett. **125**, 183002 (2020).
[12] H. Guan, S. L. Chen, X.-Q. Qi, S. Y. Liang, W. Sun, P. P. Zhou, Y. Huang, P. P. Zhang, Z.-X. Zhong, Z.-C. Yan, G. W. F. Drake, T.-Y. Shi, and K. L. Gao Phys. Rev. A **102**, 030801(R) (2020).
[13] G. W. F. Drake, in *Handbook of Atomic, Molecular, and Optical Physics*, edited by G. W. F. Drake (Springer, New York, 2006), Chap. 11.
[14] G. W. F. Drake and A. J. Makowski, J. Opt. Soc. Am. B **5**, 2207 (1988).
[15] G. W. F. Drake and Z.-C. Yan, Phys. Rev. A **46**, 2378 (1992).
[16] G. W. F. Drake, Phys. Rev. A **45**, 70 (1992).
[17] E. Riis, A. G. Sinclair, O. Poulsen, G. W. F. Drake, W. R. C. Rowley, and A. P. Levick, Phys. Rev. A **49**, 207 (1994).
[18] L. M. Wang, C. Li, Z.-C. Yan, and G. W. F. Drake, Phys. Rev. A **95**, 032504 (2017).
[19] Hylleraas wave functions, matrix elements, and total energies for all states of Li^+ up to $n = 10$ and $L = 7$ can be downloaded from http://drake.sharcnet.ca.
[20] See Supplemental Material at http://link.aps.org/supplemental/10.1103/PhysRevA.104.L060801 for extended tabulations of sensitivities for second-King plots, including low-lying states.
[21] R. A. Müller, V. A. Yerokhin, A. N. Artemyev, and A. Surzhykov, Phys. Rev. A **104**, L020802 (2021).
[22] A. Banerjee, H. Kim, O. Matsedonskyi, G. Perez, and M. S. Safronova, J. High Energy Phys. 07 (2020) 153.
[23] T. Kitahara, T. Okui, G. Perez, Y. Soreq, and K. Tobioka, Phys. Rev. Lett. **124**, 071801 (2020).
[24] P. S. B. Dev, R. N. Mohapatra, and Y. Zhang, Phys. Rev. D **101**, 075014 (2020).
[25] R. van Rooij, J. S. Borbely, J. Simonet, M. D. Hoogerland, K. S. E. Eikema, R. A. Rozendaal, and W. Vassen, Science **333**, 196 (2011).
[26] P. Cancio Pastor, L. Consolino, G. Giusfredi, P. DeNatale, M. Inguscio, V. A. Yerokhin, and K. Pachucki, Phys. Rev. Lett. **108**, 143001 (2012).
[27] P. Cancio Pastor, G. Giusfredi, P. DeNatale, G. Hagel, C. de Mauro, and M. Inguscio, Phys. Rev. Lett. **92**, 023001 (2004).
[28] M. Puchalski, A. M. Moro, and K. Pachucki, Phys. Rev. Lett. **97**, 133001 (2006).
[29] E. C. Seltzer, Phys. Rev. **188**, 1916 (1969).